

Knittable and Washable Multifunctional MXene-Coated Cellulose Yarns

Simge Uzun, Shayan Seyedin, Amy L. Stoltzfus, Ariana S. Levitt, Mohamed Alhabeab, Mark Anayee, Christina J. Strobel, Joselito M. Razal, Genevieve Dion, and Yury Gogotsi*

Textile-based electronics enable the next generation of wearable devices, which have the potential to transform the architecture of consumer electronics. Highly conductive yarns that can be manufactured using industrial-scale processing and be washed like everyday yarns are needed to fulfill the promise and rapid growth of the smart textile industry. By coating cellulose yarns with $\text{Ti}_3\text{C}_2\text{T}_x$ MXene, highly conductive and electroactive yarns are produced, which can be knitted into textiles using an industrial knitting machine. It is shown that yarns with MXene loading of ≈ 77 wt% (≈ 2.2 mg cm^{-1}) have conductivity of up to 440 S cm^{-1} . After washing for 45 cycles at temperatures ranging from 30 to 80 °C, MXene-coated cotton yarns exhibit a minimal increase in resistance while maintaining constant MXene loading. The MXene-coated cotton yarn electrode offers a specific capacitance of 759.5 mF cm^{-1} at 2 mV s^{-1} . A fully knitted textile-based capacitive pressure sensor is also prepared, which offers high sensitivity (gauge factor of ≈ 6.02), wide sensing range of up to $\approx 20\%$ compression, and excellent cycling stability (2000 cycles at $\approx 14\%$ compression strain). This work provides new and practical insights toward the development of platform technology that can integrate MXene in cellulose-based yarns for textile-based devices.

the final product.^[2–4] Therefore, the development of flexible, electrochemically and electromechanically active yarns, which can be engineered and knitted into full fabrics provide new and practical insights for the scalable production of textile-based devices.

There are various approaches in the literature to produce conductive and electrochemically active fibers and yarns. One common technique is the deposition of active material(s) onto a fiber/yarn substrate.^[9–14] This method is easily scalable and offers facile approach for incorporating various active materials into yarns. However, loading more than 30 wt% of active material onto a fiber has remained a challenge for this method, resulting in fibers with low electrical conductivity and moderate electrochemical properties.^[9,10] These results indicate the need for a more efficient coating approach that maximizes the active material loading while preventing their delamination

1. Introduction


The recent surge of interest in textile-based electronics has directed research efforts toward designing multifunctional fibers and yarns. Electrically conducting yarns are quintessential for wearable applications because they can be engineered to perform specific functions in a wide array of technologies such as energy storage, sensing, actuation, and communication.^[1–8] However, many challenges remain unaddressed regarding manufacturability of functional fibers and their integration in textiles. Current wearables utilize conventional batteries, which are bulky, uncomfortable, and can impose design limitations to

from the yarn substrate during wear and washing.^[15] Wet-spinning has also been widely used to integrate active materials such as conductive polymers,^[16–18] graphene,^[19–21] and carbon nanotubes (CNTs)^[22–25] into fibers for energy storage and sensing applications.^[17,26,27] A biscrolling technique has also been developed that produces functional yarns by trapping active materials inside CNT sheets.^[28–30] These techniques achieved high loadings (up to ≈ 97 wt%) of active materials into fibers or yarns.^[29] However, functional fibers or yarns produced using these methods seldom offer the mechanical properties required by textile processing and can be challenging to scale-up. In the context of wearables, manufacturability of the yarns

S. Uzun, Dr. S. Seyedin, A. S. Levitt, M. Alhabeab, M. Anayee, Prof. Y. Gogotsi
A. J. Drexel Nanomaterials Institute
Department of Materials Science and Engineering
Drexel University
Philadelphia, PA 19104, USA
E-mail: gogotsi@drexel.edu

Dr. S. Seyedin, Prof. J. M. Razal
Institute for Frontier Materials
Deakin University
Geelong, VIC 3216, Australia
A. L. Stoltzfus, Prof. G. Dion
Center for Functional Fabrics
Drexel University
Philadelphia, PA 19104, USA

C. J. Strobel
Department of Electrical and Computer Engineering
Drexel University
Philadelphia, PA 19104, USA

 The ORCID identification number(s) for the author(s) of this article can be found under <https://doi.org/10.1002/adfm.201905015>.

DOI: 10.1002/adfm.201905015

is crucial because high electrical conductivity and electrochemical performance do not necessarily correspond to the feasibility of industrial-scale knitting or weaving processes. When considering the use of functional yarns in truly wearable applications, washability also becomes important. The ability to withstand prolonged exposure to aqueous environments is necessary for practical applications because textiles undergo various washing cycles after use.

The above limitations led us to develop our understanding of the fabrication of knittable, washable, and highly conductive yarn electrodes using MXenes. MXenes are a large family of 2D transition metal carbides and nitrides which have a general formula of $M_{n+1}X_nT_x$, where M is a transition metal, X is carbon and/or nitrogen with $n = 1, 2$, or 3, and T_x denotes the surface termination ($-OH$, $-O$, and $-F$). MXenes have attracted significant attention due to their high electrical conductivity (up to $10\,000\text{ S cm}^{-1}$ as a thin film)^[31] and excellent volumetric capacitance (up to 1500 F cm^{-3}).^[32] Their hydrophilic surface, due to the presence of abundant functional groups, makes them suitable for solution processing by spray-coating, vacuum-assisted filtration, printing, and painting from aqueous solutions.^[33] Ti_3C_2 MXene (referred to as Ti_3C_2 for simplicity) has demonstrated exceptional cation intercalation and pseudocapacitive behavior, which is ideal for energy storage applications.^[34–37] Ti_3C_2 MXene is also biocompatible^[38,39] and does not present a risk in case of contact with skin. Environmental degradation or incineration of Ti_3C_2 produces titanium dioxide (TiO_2) and carbon dioxide (CO_2), which do not present threats to the environment.

By using Ti_3C_2 as an active material, we employed a simple two-step dipping and drying procedure and converted conventional cellulose-based yarns such as cotton, bamboo, and linen into yarn electrodes. These MXene-coated yarns demonstrate three orders of magnitude increase in electrical conductivity and one order of magnitude increase in electrochemical performance when compared to carbon materials.^[14] By optimizing the coating process and carefully choosing appropriate MXene sheet size at each step of the coating process, we achieve yarns with a high loading of 78 wt% MXene. We demonstrate that these yarns can be washed at temperatures ranging from 30 to 80 °C for 45 washing cycles and with minimal decrease in conductivity. We further show that for the first time, these yarns can be knitted into various stitch patterns using an industrial scale knitting machine, which were only achieved by simulation in previous reports (Figure 1). The electrochemical performance of MXene-coated cotton yarns shows that they have the potential to power wearable electronics as yarn supercapacitor (YSC) devices. We also demonstrated that the knitted MXene-coated yarns can be used to make a flexible and wearable capacitive pressure sensor. While the scope of this work focuses on MXene-coated cellulose-based yarns and demonstration of energy storage and pressure sensing applications, these yarns offer electrical and electrochemical properties that can meet the requirements of other applications such as in energy harvesting, other types of sensors (e.g., strain, moisture, and temperature), antennas, heaters, and electromagnetic interference (EMI) shielding. Such functional yarns offer a platform technology, which utilizes these conformal yarns to enable development of various types of textile-based devices.

2. Results and Discussion

2.1. Production of Conductive MXene-Coated Cellulose-Based Yarns

The initial step in producing the MXene-coated yarns begins with solution processing of MXene into homogenous dispersions (Figure 2a). X-ray diffraction (XRD) results indicated the successful etching of Al layers and exfoliation of MXene by the expansion and disorder of the interlayer spacing according to the (002) peak (Figure S1a, Supporting Information). The disappearance of the (014) peak in the resulting Ti_3C_2 films indicated there is no residual MAX phase. Transmission electron microscopy (TEM) studies confirmed the synthesis of delaminated MXene nanosheets (small MXene flakes, S- Ti_3C_2 , Inset of Figure 2b and the large MXene flakes, L- Ti_3C_2 , Figure S1b, Supporting Information). Figure S1c,d (Supporting Information) shows an atomic force microscopy (AFM) images of S- Ti_3C_2 and L- Ti_3C_2 MXene flakes, respectively. The concentration of the MXene dispersions used during dipping was between 25–30 mg mL⁻¹. MXene flakes are negatively charged and hydrophilic due to their surface functional groups (e.g., $-O$, $-OH$, and $-F$). As shown in Figure 2b, the zeta potential of the Ti_3C_2 MXene flakes was measured as -56 mV at pH 6.8. When hydrophilic cotton yarns were dipped into negatively charged MXene dispersions, MXene flakes attached to the surface of cotton fibers. As a result, strong electrostatic interactions were established between MXene flakes and cotton fibers. The XRD pattern for Ti_3C_2 -coated cotton yarn shows



Figure 1. Seamlessly knitted MXene-coated cellulose-based yarns. Concept illustration of a garment integrated with energy storage and harvesting device with a capacitive pressure sensor. Insets show actual device prototypes comprising of a) knitted energy storing fabric with alternating MXene-coated cotton yarn (black) and a nonconductive commercial viscose yarn (green). b) Knitted energy harvesting fabric with alternating MXene-coated linen yarn (black) and a commercial Teflon yarn (brown) can be placed strategically to harvest energy from body movements. c) Capacitive pressure sensor device knitted with MXene-coated bamboo yarn, where the device can sense different applied pressures ranging from low to high.

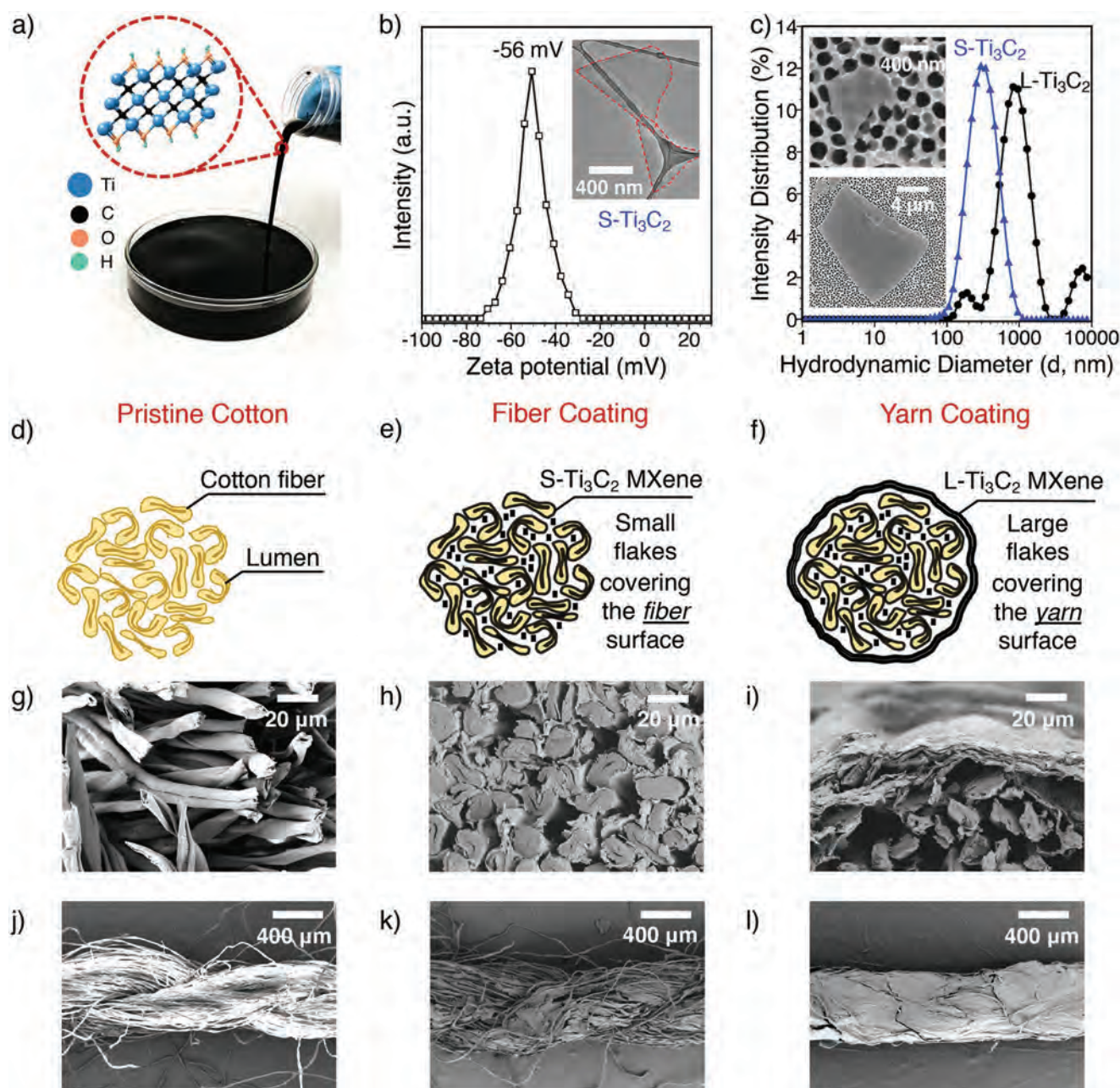


Figure 2. Characterization of Ti_3C_2 MXene dispersions. a) Digital photograph of ≈ 100 mL of MXene dispersion (≈ 20 – 25 mg mL $^{-1}$) in a petri dish with a schematic of the atomic structure of Ti_3C_2 MXene flake. b) Zeta potential (graph) at pH 6.8 and transmission electron microscopy (TEM) image (inset) of S- Ti_3C_2 MXene flakes. c) Flake-size distribution of as-synthesized (L- Ti_3C_2) and probe sonicated (S- Ti_3C_2) MXene dispersions. The size is represented as hydrodynamic diameter (d , nm) in nanometers. Insets: Scanning electron microscopy (SEM) images of S- Ti_3C_2 (Top) and L- Ti_3C_2 (Bottom) MXene flakes. Two-step coating process of highly conductive MXene-coated cotton yarns. First coating step (fiber coating) requires using S- Ti_3C_2 MXene flakes, which enables MXene penetration into the fiber level. Second coating step (yarn coating) uses L- Ti_3C_2 MXene flakes to cover the yarn surface to provide high conductivity. The schematic illustration of the cross-section of cotton yarn d) pristine, e) coated with S- Ti_3C_2 MXene flakes, f) coated with S- Ti_3C_2 and L- Ti_3C_2 MXene flakes. Cross-section SEM images of g) pristine cotton fibers, h) cotton fibers coated with S- Ti_3C_2 MXene flakes, i) cotton yarn after being coated with S- Ti_3C_2 and L- Ti_3C_2 MXene flakes. SEM images of the cotton yarn surface j) pristine, k) coated with S- Ti_3C_2 MXene flakes, and l) coated with S- Ti_3C_2 and L- Ti_3C_2 MXene flakes.

signatures of both Ti_3C_2 MXene and cotton peaks (Figure S1, Supporting Information). In order to increase the overall active material loading during the dip-coating process, MXene dispersions with two different flake size distributions were used in this study: as-synthesized (L- Ti_3C_2 MXene) and probe sonicated

(S- Ti_3C_2 MXene). According to the dynamic light scattering (DLS) results (Figure 2c), L- Ti_3C_2 MXene dispersions were primarily composed of large flakes with an average particle size of 1 μm , whereas the S- Ti_3C_2 MXene dispersions were composed of nanoscale-sized flakes with an average particle size

of 340 nm. Scanning electron microscopy (SEM) images of S-Ti₃C₂ and L-Ti₃C₂ MXene flakes (Inset of Figure 2c) are in agreement with the DLS data. It has been shown that L-Ti₃C₂ MXene flakes result in higher electrical conductivity compared to S-Ti₃C₂ MXene flakes,^[40] which is most likely due to less interfacial resistance between L-Ti₃C₂ MXene flakes. Films made by filtering L-Ti₃C₂ MXene flakes showed higher electrical conductivity of $\approx 9490 \text{ S cm}^{-1}$, whereas the films produced by filtering S-Ti₃C₂ MXene flakes resulted in electrical conductivity of $\approx 4080 \text{ S cm}^{-1}$.

Three different approaches for producing conductive yarns with MXene dispersions were studied: 1) coating with S-Ti₃C₂ MXene, 2) L-Ti₃C₂ MXene, and 3) combination of small and large flakes. The pristine cotton yarn consists of twisted cotton fibers, which have a kidney-shaped cross-section with a hollow core (lumen) as illustrated in Figure 2d. Unlike most synthetic yarns, cotton fibers have a rough surface (Figure 2g), which is ideal for nanoparticle adhesion. The first coating process consisted of using only S-Ti₃C₂ MXene dispersions to allow for small MXene flakes to infiltrate between individual fibers (Figure 2e,h). Using this coating method, the cotton yarn retained its flexibility. The conductivity of S-Ti₃C₂-coated cellulose-based yarns with MXene loadings of 0.6 mg cm^{-1} was between 30 and 50 S cm^{-1} , which is sufficient for a variety of applications such as pressure and strain sensing. The second coating method utilized L-Ti₃C₂ MXene dispersions to achieve MXene coating only on the surface of the yarn. When only MXene dispersions with large flakes were used to coat the yarns, the formation of MXene coating on the yarn surface prevented the further infiltration of MXene flakes into the internal yarn structure, thereby leaving the individual fibers closer to the center uncoated. The conductivity of L-Ti₃C₂-coated cellulose-based yarns ranges from 60 to 85 S cm^{-1} (MXene loading of 0.6 mg cm^{-1}), which is higher than the conductivity of the yarns coated only with S-Ti₃C₂ MXene flakes. Even though higher conductivity is achieved with L-Ti₃C₂-coated cellulose-based yarns, the yarns become less flexible. Notably, as the L-Ti₃C₂ MXene loading increased up to 0.6 mg cm^{-1} , MXene coating easily delaminated from the yarn surface upon forming loops during knitting. Thus, the yarns coated with only L-Ti₃C₂ MXene flakes were not integrated into functional devices.

In order to balance the flexibility and the conductivity of the MXene coated yarns, we first infiltrated the internal yarn structure with S-Ti₃C₂ MXene in order to coat the individual fibers before finally coating the external yarn with L-Ti₃C₂ MXene. This approach, the two-step coating process, maximizes the MXene loading by coating both on the fiber and the yarn level. Detailed fabrication process of the MXene-coated cellulose-based yarns can be found in Video S1 (Supporting Information). In order to maximize MXene loading on the yarn, the fibers were first saturated with S-Ti₃C₂ MXene flakes before coating with L-Ti₃C₂ MXenes to cover the yarn surface (Figure 2f,i). This coating approach could be ideal for yarn supercapacitor applications since the capacitance has been reported to be MXene loading dependent.^[10] The cotton yarn surface after coating with only S-Ti₃C₂ (Figure 2k) remained similar to the pristine cotton (Figure 2j) in terms of flexibility because majority of the small flakes infiltrated into the fiber. On the other hand, the twist became no longer visible after coating with both S-Ti₃C₂ and

L-Ti₃C₂ MXene dispersions (Figure 2l), which created a continuous conductive pathway along the yarn surface. The yarns produced via two-step dip coating process were not as flexible as the yarns coated with only S-Ti₃C₂ MXene dispersions. However, they demonstrated easier knittability and less flaking compared to the yarns coated with only L-Ti₃C₂ MXene dispersions. This is most likely due to a more balanced weight distribution between the center and the outside of the yarn achieved with the two-step dip coating process, where the presence of S-Ti₃C₂ MXene flakes at the internal yarn structure helped to balance the yarn's weight compared to only the presence of cotton fibers when the yarn surface only coated with L-Ti₃C₂ MXene dispersions. The same coating process was also applied to bamboo and linen yarns to demonstrate the adaptability of this method to other cellulose-based yarns. More detailed cross-sectional SEM images of the pristine and MXene-coated cotton, bamboo, and linen yarns are shown in Figure S2 (Supporting Information). The MXene-coated yarns were dried thoroughly in air and subsequently placed in a vacuum desiccator prior to further evaluation.

To determine the mass loading of MXene, each yarn was weighed before and after dip-coating with MXene. The masses were averaged from three skeins with 200 cm length in order to account for mass variation along the length of the yarn. By following the two-step coating procedure, the active mass loading of up to 78 wt% (2.5 mg cm^{-1}) could be achieved with cotton yarns. MXene-coated bamboo and linen yarns showed similar MXene loadings of $\approx 75 \text{ wt\%}$ (2.2 mg cm^{-1}) and $\approx 77 \text{ wt\%}$ (2.2 mg cm^{-1}), respectively. To the best of our knowledge, the active mass loading of $\approx 78 \text{ wt\%}$ deposited on the yarns is the highest reported value in the literature for a facile, yarn dip-coating approach.

Investigation of the changes in resistance and conductivity of the MXene-coated cellulose-based yarns with length (Figure S3a, Supporting Information) revealed that the resistance increased linearly as a function of yarn length, thus the conductivity remained unchanged when the yarn length increased from ≈ 1 to ≈ 210 cm. At the highest MXene loading of 78 wt%, the conductivity of the MXene-coated cotton yarn reached $198.5 \pm 1.4 \text{ S cm}^{-1}$ ($1.7 \pm 0.2 \Omega \text{ cm}^{-1}$, yarn diameter $\approx 610 \mu\text{m}$). While bamboo yarns with 75 wt% MXene loading exhibited similar conductivity values with MXene-coated cotton yarns, the conductivity of the linen yarns with 77 wt% MXene loading reached $440.3 \pm 0.9 \text{ S cm}^{-1}$, which is ≈ 2.2 times higher than MXene-coated cotton and bamboo yarns. Since linen yarns possess the smallest diameter ($\approx 425 \mu\text{m}$) among all examined yarns ($\approx 610 \mu\text{m}$ for cotton and $\approx 570 \mu\text{m}$ for bamboo), the improved conductivity of the MXene-coated linen yarns can be attributed to the ≈ 1.8 times higher MXene loading per unit volume of the linen yarn compared to cotton and bamboo yarns. Moreover, linen fibers (60–120 cm) are the longest fibers studied in this paper when compared to cotton (1–4 cm) and bamboo (5–8 cm) fibers. Similar to S-Ti₃C₂ versus L-Ti₃C₂ MXene flakes, longer fibers infiltrated with MXene flakes help to decrease the overall interfacial resistance along the yarn length by creating more effective conduction paths. Mechanical testing of MXene-coated cellulose-based yarns at the maximum active material loading (75–78 wt%) shows that MXene addition also reinforces the yarn, improving the mechanical

properties (Figure S3b, Supporting Information). For instance, at 78 wt% MXene, the cotton yarn showed a Young's modulus of 5.0 ± 0.3 GPa and a tensile strength of 468.4 ± 27.1 MPa, which were $\approx 7\%$ and $\approx 40\%$ higher than those of the pristine cotton yarns, respectively. Moreover, MXene-coated cotton yarn (78 wt% MXene loading) can form a knot (Figure S3c, Supporting Information), indicating good flexibility and knittability. Thus, coating of cellulose-based yarns with Ti_3C_2 MXene dispersions resulted in flexible and mechanically stable yarns that offer good electrical conductivity and high active material loading for a variety of promising applications.

2.2. Knittability of MXene-Coated Cellulose-Based Yarns

We investigated the knittability of the MXene-coated cellulose-based yarns, including cotton, linen, and bamboo into full fabrics on an industrial machine using different stitch patterns. Knitting, the intermeshing of yarn loops to form a textile, was chosen due to its flexibility in programming and rapid prototyping. During industrial knitting process, the yarns are subjected to uniaxial tensile and bending stresses, making the overall stress much higher in comparison to hand knitting. Knitting cotton yarns coated with active materials with industrial machines was not possible for a long time as discussed in previous literature.^[14] One of the reasons is that the cotton fibers are more likely to pull apart from each other while under tension during knitting since they consist of shorter fibers (1–4 cm) in comparison to other cellulose-based yarns (5–8 cm

for bamboo and 60–120 cm for linen).^[14] The MXene-coated yarns are stronger and less flexible compared to their pristine counterparts. We addressed their reduced flexibility (after coating) by optimizing the stitch patterns through extensive parametric studies.

Here, we successfully knitted MXene-coated cotton and other cellulose-based yarns into swatches (fabric samples with $60 \text{ mm} \times 65 \text{ mm}$ in total area and $16 \text{ mm} \times 26 \text{ mm}$ in active area) and investigated different stitch patterns (geometric construction of the knitted loops) including single jersey (Figure 3a), half-gauge (Figure 3b), and interlock (Figure 3c). The stitch pattern dictates how the yarns are inter-looped to create different knit structures. Single jersey is the most common fabric type and simplest loop structure among knitted textiles. However, it is not necessarily the ideal stitch pattern when it comes to knitting the coated yarns since these yarns exhibit lower flexibility compared to their pristine states. In jersey knits, the loops are formed using every needle adjacent to each other on the needle bed. This can result in yarn-to-yarn rubbing and breakage due to a smaller bending radius of the yarn during knitting (Figure 3d). To prevent the yarn breakage, a half-gauge pattern can be knitted. Half-gauge knit uses every other needle on the bed in each machine pass, resulting in a more porous fabric (Figure 3e). The interlock pattern (Figure 3f), also uses every other needle but knits all needles in two passes. Odd needles (denoted with asterisks) are knitted in the first machine pass and the even needles (denoted with triangles) are knitted during the second pass of the sequence. The interlock pattern (Figure 3f) results in a fabric closer in density to single

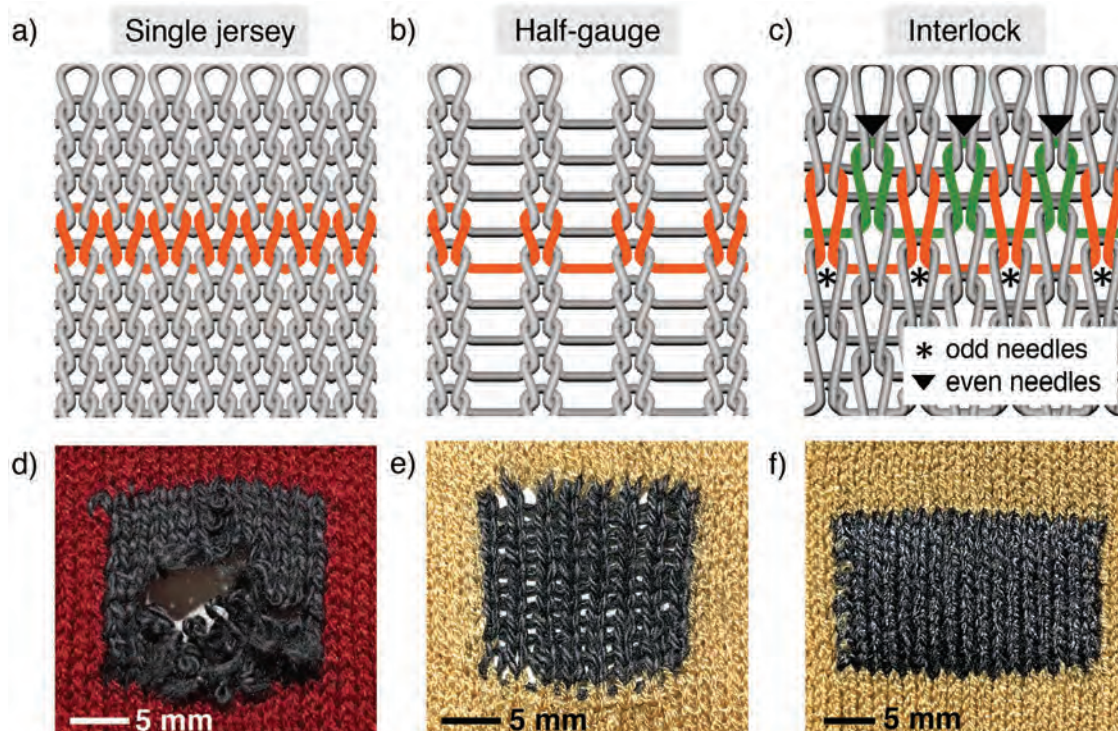


Figure 3. Different stitch patterns commonly used in knitted fabrics. a) Single jersey. b) Half gauge. c) Interlock. d) Unsuccessful attempt to knit MXene-coated cotton yarn (black) in single-jersey pattern. e) MXene-coated cotton yarn knitted with half-gauge pattern resulted in a porous fabric. f) MXene-coated cotton yarn knitted with interlock pattern resulted in a dense fabric.

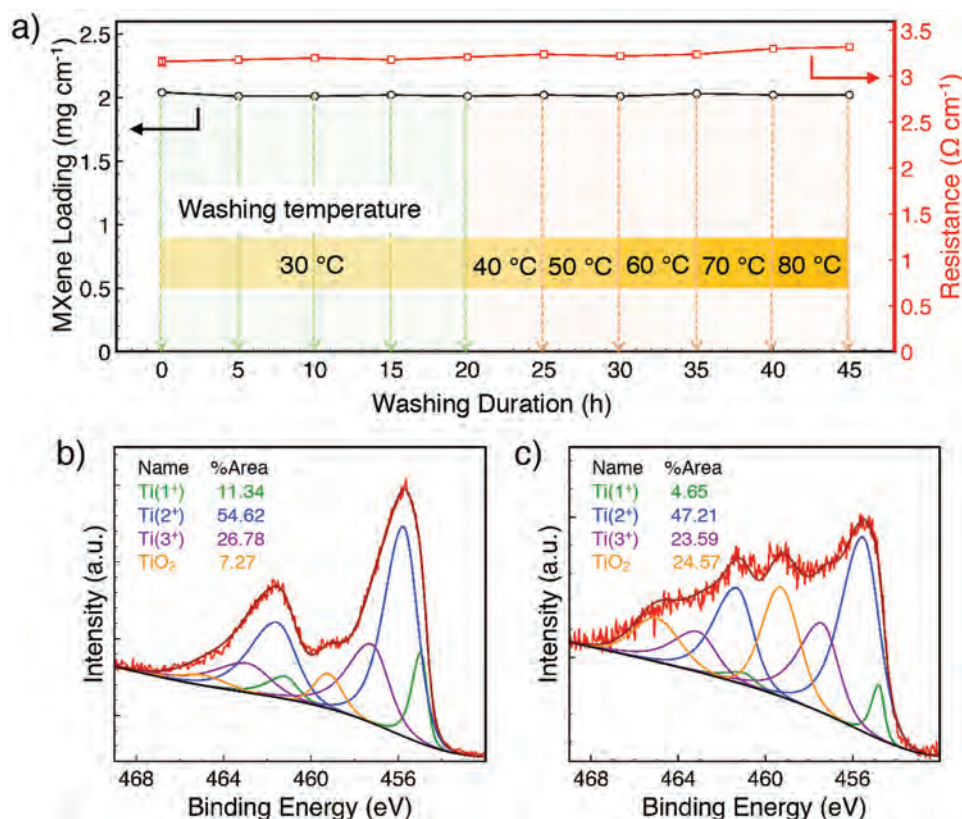


Figure 4. Washing durability performance of MXene-coated cotton yarns ($\approx 2 \text{ mg cm}^{-1}$ MXene loading) under various washing temperatures and times. a) The change in the MXene loading and the linear resistance as a function of washing temperature ranging from 30 to 80 °C. Ti2p XPS spectra of b) unwashed MXene-coated cotton yarn and c) washed MXene-coated cotton yarn after 3 min of sputtering. The yarns were washed for 20 washing cycles at 30 °C and 5 washing cycles at temperatures ranging from 40 to 80 °C.

jersey and is denser compared to the half-gauge pattern. Thus, utilization of half-gauge and interlock stitch patterns increased the space between each line of the loops and reduced the yarn-to-yarn friction and yarn breakage. The ability to knit MXene-coated cellulose-based yarns with different stitch patterns allowed us to control the fabric properties such as porosity and thickness for various applications. Understanding the properties and the limitations of conductive yarns enabled us to adjust the stitch patterns and the corresponding knitting parameters in order to knit these yarns.

2.3. Washability of MXene-Coated Cellulose-Based Yarns

The ability of conducting fibers to withstand prolonged exposure to aqueous environments is critical for use in wearable applications. The impact of washing was studied using Ti_3C_2 -coated cotton yarns produced by the two-step dip-coating process. S- Ti_3C_2 MXene was used to coat the individual fibers in the internal yarn structure, then L- Ti_3C_2 MXene was used to coat the external yarn surface. The outer MXene coating on the yarn surface was $15.2 \pm 0.8 \mu\text{m}$ based on the cross-sectional SEM images. The MXene loading remained relatively unchanged ($<1\%$ decrease) after 45 h of washing cycles at temperatures ranging from 30 to 80 °C, as shown in Figure 4a. This is due to the strong interactions between MXene flakes so that even

vigorous shaking did not redisperse the flakes as shown in free-standing films.^[35] MXene-coated cotton yarns showed minimal change in linear electrical resistance after 20 washing cycles at 30 °C. As the washing temperature increased from 30 to 80 °C, the linear resistance increased only by $\approx 3\%$. SEM images of the unwashed (Figure S4a, Supporting Information) and washed (Figure S4b, Supporting Information) MXene-coated cotton yarns after 45 washing cycles revealed very little material loss even after 45 h at elevated temperature in water. The washed MXene-coated cotton yarns demonstrated similar mechanical properties to the unwashed MXene-coated yarns with tensile strength of $460.1 \pm 25.2 \text{ MPa}$, Young's modulus of $4.8 \pm 0.2 \text{ GPa}$, and failure at strain value of 0.0844 ± 0.004 . This result is the first to demonstrate the negligible detrimental effect of washing MXene-coated yarns on their mechanical properties.

X-ray photoelectron spectroscopy (XPS) was used to investigate if the washing process resulted in oxidation or degradation of MXene. XPS is inherently a surface sensitive technique due to the shallow escape depth of the photoelectrons generated from the material, therefore, the spectra gathered are indicative of only the outer $<15 \text{ nm}$ surface layer. Figure 4b shows that the MXene in the unwashed fibers exhibited very low degree of oxidation whereby $\approx 7.3 \text{ at\%}$ of Ti in MXene was in the form of Ti^{4+} (indicative of TiO_2) which is the product of Ti_3C_2 MXene oxidation. After washing the yarns at 30 °C for 20 washing cycles followed by 25 washing cycles from

40 to 80 °C, the MXene in the thin outer surface layer was oxidized with the Ti^{4+} comprising ≈ 43.6 at% (Figure S4c, Supporting Information). After sputtering for just 3 min, the measured degree of oxidation decreased to ≈ 24.6 at% (Figure 4c). Bulk properties, such as electrical conductivity, are often governed by the overall state of the material. The resistance of the MXene-coated cotton yarn increased by less than 5% after washing at temperatures ranging from 30 to 80 °C for 45 washing cycles, as shown in Figure 4a. Partial surface oxidation (<1 μm in thickness^[41] compared to ≈ 15.2 μm in thickness of the external MXene layer) does not seem to significantly affect the overall conductivity of the yarns. The remaining MXene flakes in both the fiber and the yarn levels are able to provide similar conductivity values to unwashed MXene-coated cotton yarn. The summary of the high-resolution $\text{Ti}2\text{p}$ XPS region is provided in Table S1 in the Supporting Information for unwashed and washed MXene-coated cotton yarns before and after sputtering. These results further support our findings of the stability of MXene-coated cotton yarns under harsh environments. Unlike the colloidal MXene dispersions,^[42–44] once the MXene flakes are assembled and dried, there are no more reactive pathways for oxidation because additional water cannot easily rehydrate the structure. As a result, the exposure to water and temperature does not seem to affect the overall electrical conductivity of the MXene-coated cotton yarns as observed in the case of assembled MXene flakes in films.^[42,45]

2.4. Electrochemical Properties of MXene-Coated Cotton Yarns

Electrochemical performance of MXene-coated cotton yarns was evaluated using a standard three-electrode setup with 1 M H_2SO_4 electrolyte to assess the feasibility of using these yarns for energy storage applications. Cotton yarn with 78 wt% (2.5 mg cm^{-1}) of MXene loading was used as the working electrode without any current collector during the test. Using cyclic voltammetry (CV), the stable potential range for the MXene-coated cotton yarns was identified to be between -0.55 and 0.25 V versus Ag/AgCl (Figure 5a). The representative CV and galvanostatic charge–discharge (GCD) curves of the MXene-coated cotton yarns at different scan rates and current densities were shown in Figure 5b,c, respectively. The CV curves demonstrated a quasi-rectangular shape with close to $\approx 100\%$ Coulombic efficiency under anodic potential at all scan rates indicating the capacitive behavior of MXene-coated cotton yarns. An increased capacitance under high cathodic potentials is due to H^+ induced redox behavior of Ti_3C_2 (pseudocapacitance).^[32,46] The GCD curves at different current densities, are highly symmetrical even at high discharge current density of 24 mA cm^{-1} . The specific capacitances as a function of scan rates were determined using CV curves as shown in Figure 5d. The specific capacitance decay as a function of scan rate was most likely to be due to the diffusion limitations of the ionic transport. Similar intercalation/deintercalation rate limitation was also observed in case of thick planar MXene electrodes.^[32,47]

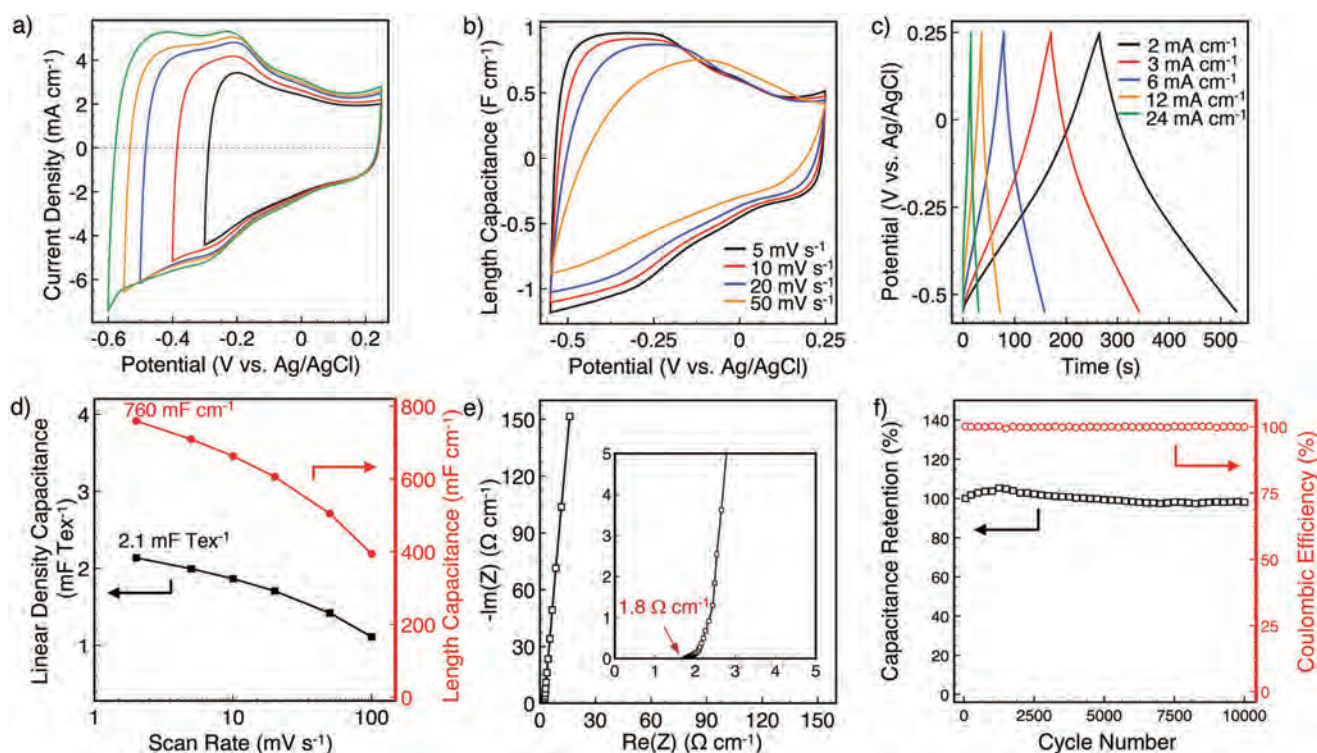


Figure 5. Electrochemical performance of MXene-coated cotton yarns with 78 wt% (2.5 mg cm^{-1}) MXene loading using a three-electrode cell in 1 M H_2SO_4 . a) Cyclic voltammetry (CV) curves (5 mV s^{-1}) at various operation potentials. b) CV curves of MXene-coated yarns at various scan rates. c) Galvanostatic charge–discharge (GCD) curves at various current densities. d) Rate capability of length and linear density capacitance of MXene-coated cotton yarns. e) Normalized Nyquist plot based on the length of the yarn. f) Cyclic stability of the MXene-coated cotton yarn during 10 000 cycles at a current density of 30 mA cm^{-1} .

The MXene-coated cotton yarn displayed a length capacitance (C_L) of $\approx 759.5 \text{ mF cm}^{-1}$ at 2 mV s^{-1} . The areal capacitance (C_A) and volumetric capacitance (C_V) values were also calculated from CV curves at 2 mV s^{-1} as $\approx 3965.0 \text{ mF cm}^{-2}$ and $\approx 260.0 \text{ mF cm}^{-3}$, respectively. Gravimetric capacitance (C_G) is dependent on the thickness and density of the electrodes as well as weight of the other components, which results in unreliable comparison between different supercapacitors.^[48,49] However, mass is an important parameter and cannot be neglected. Both the gravimetric (mass) and the linear, areal, or volumetric capacitances need to be considered when evaluating the capacitance performance.^[3,15] Tex, mass of the yarn in grams per 1000 m, is a common metric used in the textile industry.^[50] It takes into consideration both the mass and the length of the yarns to avoid the faulty assumption of yarns being perfect cylinders with fixed diameters. The linear density of the cotton yarns at 2.5 mg cm^{-1} MXene loading (mass of the pristine cotton yarn $\approx 0.7 \text{ mg cm}^{-1}$) was measured as 320 Tex. Thus, the linear density capacitance of the electrode (C_{Tex}) was 2.1 mF Tex^{-1} at 2 mV s^{-1} . To the best of authors' knowledge, the cotton yarns with 78 wt% MXene loading exhibited the highest specific length capacitance among the cellulose-based yarn-shaped supercapacitors reported to date.^[14,51–53]

Electrochemical impedance spectroscopy (EIS) was conducted to understand the charge transfer and ion transport properties of the MXene-coated cotton yarns. As shown in Figure 5e, the equivalent series resistance (ESR) was calculated as $1.8 \Omega \text{ cm}^{-1}$ from the high frequency intercept of the Nyquist plot. MXene-coated cotton yarns showed a short Warburg region with a 45° angle, which indicated good ion diffusion efficiency, and a linear behavior in the low-frequency region, demonstrating close to the ideal capacitive behavior. As shown in Figure 5f, MXene-coated cotton yarns exhibited excellent cyclic stability with 100% Coulombic efficiency after 10 000 cycles at a current density of 30 mA cm^{-1} . It should be noted that the MXene coated cotton yarn electrode has not been precycled prior to the cyclability test and the $\approx 5\%$ increase in capacitance stabilized back to 100% retention after ≈ 2000 cycles. This result shows that for practical applications, the textile supercapacitors built using MXene-coated cotton electrodes need to be preconditioned prior to use. SEM images (Figure S5, Supporting Information) of the MXene-coated cotton yarns before and after 10 000 cycles show that the morphology of the yarns as well as the MXene coating remained almost unchanged.

The electrochemical results indicate that MXene-coated cotton yarns can be a potential candidate in powering wearable electronics. They can be incorporated into symmetric yarn supercapacitors to offer sufficient energy and power for a variety of applications. To demonstrate this, yarn supercapacitors were fabricated using a symmetric device configuration where both of the electrodes had the same amount of MXene loading. The electrodes were separated by a polyvinyl alcohol (PVA)– H_2SO_4 gel electrolyte. The voltage window was kept at 0.6 V to prevent the oxidation of Ti_3C_2 MXene as suggested by previous studies.^[54,55] From the CV curves shown in Figure S6a (Supporting Information), the specific capacitance values of the device (at 2 mV s^{-1}) were calculated as C_L of $\approx 306.9 \text{ mF cm}^{-1}$ (0.6 mF Tex^{-1}), C_A of $\approx 1865.3 \text{ mF cm}^{-2}$, and

C_V of $\approx 142.4 \text{ mF cm}^{-3}$. The GCD curves (Figure S6b, Supporting Information) are highly symmetric at all current densities investigated with negligible iR drop. The rate handling of the symmetric yarn supercapacitor device shown in Figure S6b (Supporting Information) can be improved further by using a yarn electrode with smaller diameter, which would reduce the overall thickness of the device and improve the ion diffusion at higher scan rates. The Nyquist plot (Figure S6d, Supporting Information) showed nearly vertical behavior at all frequencies, suggesting fast ion diffusion with an estimated ESR value of $7.1 \Omega \text{ cm}^{-1}$. The yarn supercapacitor device showed a long-term capacitance retention of $\approx 100\%$ after 10 000 charge-discharge cycles while maintaining 100% Coulombic efficiency (Figure S6e, Supporting Information) when tested with GCD cycles at 5 mA cm^{-1} . Further increase in the voltage window and energy storage can be achieved by using organic electrolyte.^[56] The stability and performance of free-standing yarn supercapacitor devices (5 cm long) were also tested under bending cycles at various bending angles as shown in Figure S6f (Supporting Information). The device demonstrated stable response with a $\approx 100\%$ capacitance retention after 1000 cycles when bent at 90° . The performance of the device remained stable when repeated deformations were applied during the test.

2.5. Knitted Capacitive Pressure Sensor Device

To demonstrate multifunctionality of MXene-coated yarns, we also used them to make a textile pressure sensor device. Since MXene-coated cotton yarns were used to demonstrate the feasibility of energy storage applications, MXene-coated bamboo yarns have been chosen for the pressure sensor device assembly. We knitted MXene-coated bamboo yarns (MXene loading 0.6 mg cm^{-1}) into a rectangular swatch (16 mm by 26 mm) surrounded by a knitted viscose yarn using interlock stitch (Figure 6a). The capacitive textile sensor device was then prepared by carefully placing two identical knitted swatches on top of each other with a dielectric layer of thin nitrile rubber sandwiched in between. The electromechanical measurement of the textile sensor showed that the capacitance (C) increased with compression strain (Figure 6b) and applied stress (Figure S7a, Supporting Information), and returned to initial value (C_0) when released. The capacitance response of the sensor as a function of various magnitudes of cyclic compression strains (Figure 6c) showed that the textile sensor was able to respond to a wide range of compression strains (ϵ) from 2.8% to 19.7%, equivalent to pressures of 0.002 and 66 kPa (per whole sensor area, not considering textile porosity), respectively. Notably, the relative change in capacitance ($\Delta C/C_0$) showed a linear relationship with the magnitude of compression strain, indicating the linearity of the sensing response (Figure 6d). Fitting a linear line to $\Delta C/C_0$ versus ϵ data revealed a slope of 6.02. This slope corresponds to the gauge factor (GF) of the sensor, defined as $\Delta C/\epsilon C_0$. GF is an important sensing metric as it determines the sensitivity of the sensor device. This GF is comparable to other capacitive textile-based pressure sensors^[57,58] indicating the high sensitivity of the knitted MXene-coated yarn pressure sensor device. When repeatedly compressed and relaxed for 2000 cycles at 14.1% strain, the

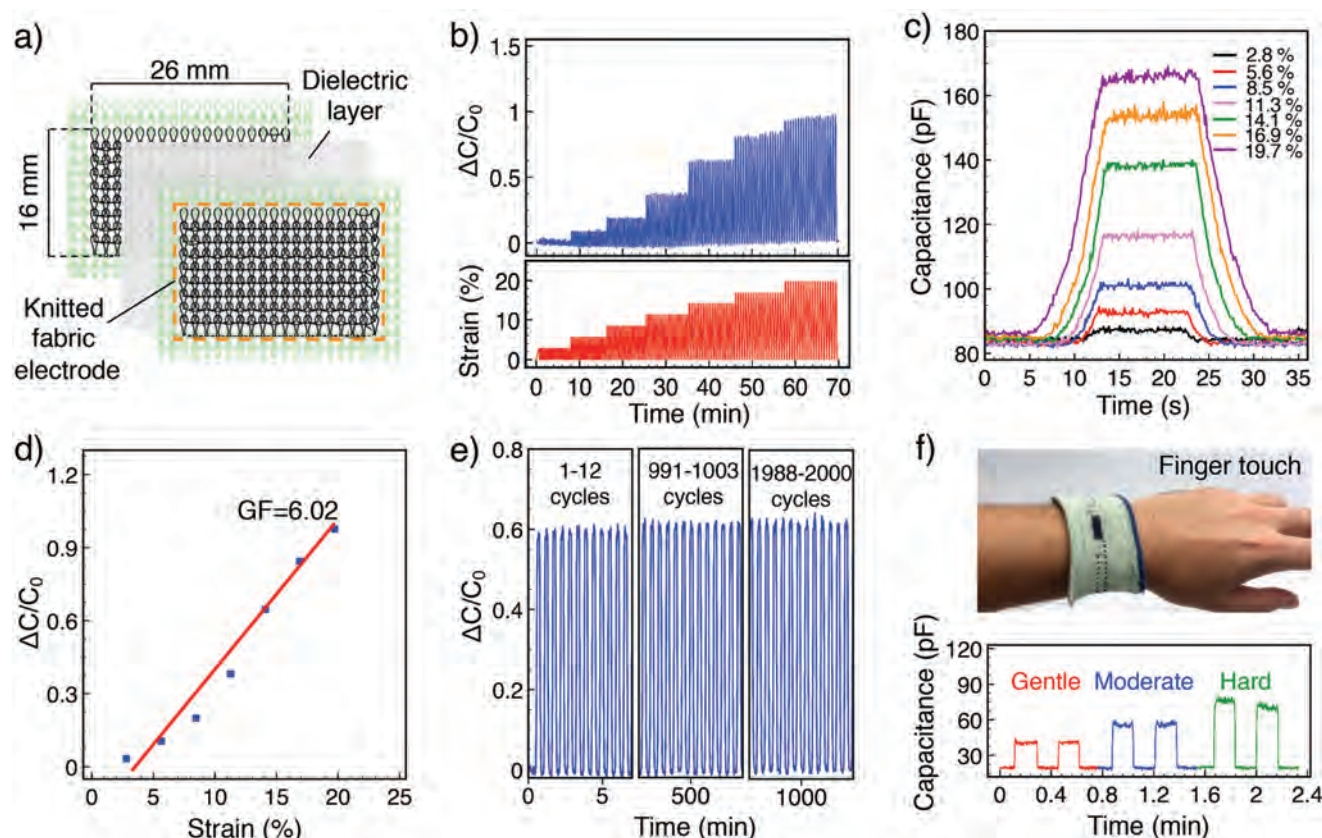


Figure 6. Evaluation of sensing performance of the capacitive knitted pressure sensor device. a) Schematic representation of the capacitive pressure sensor (active area—16 mm × 26 mm) assembled by using two knitted fabric electrodes and a dielectric layer. b) Electromechanical behavior of the knitted sensor. The applied strain is incrementally increased from 2.8 to 19.7%. Each cyclic deformation is repeated 20 times. c) Capacitance as a function of time at different compression strains ranging from 2.8 to 19.7%. The hold time is 10 s. d) Relative capacitance changes of the sensor at various strains. Gauge factor (GF) is derived from the linear fit. e) Cyclic stability of the sensor based on relative capacitance change at 14.1% strain for 2000 cycles. f) Top: digital photo of the knitted pressure sensor button (active area—16 mm × 5 mm). Bottom: capacitance output of the sensor when a gentle, moderate, or hard pressure is applied to the device by a finger.

capacitive response of the textile device remained constant (Figure 6e), indicating excellent cyclic stability. This long-term sensing stability demonstrates that the sensor's response is reproducible.

We also prepared a proof-of-concept capacitive pressure sensor button (Figure 6f) by knitting the MXene-coated yarn into fully functional device, i.e., two textile electrodes and a sandwiched dielectric layer, in one step using an industrial-scale knitting machine (see the Experimental Section for detail). The knitted pressure sensor button was capable of sensing various levels of finger pressures and weights. For instance, the capacitance response of the sensor increased approximately two, three, and four times its initial value when gentle, moderate, and hard pressures were applied, respectively (Figure 6f). Moreover, 20% and 50% increases in the capacitance response were observed when 5 and 20 g weights were placed on the textile device, respectively (Figure S7b, Supporting Information). These examples show that the knitted fabric sensor is capable of distinguishing various levels of applied pressures and may be used in practical applications. The performance of the knitted pressure sensor can be further improved in the future by changing the yarn type, stitch pattern, active material

loading, and the dielectric layer to result in higher capacitance changes under applied pressure to achieve more reliable devices for wearable applications.

3. Conclusion

This work introduced a simple two-step dip-coating process using colloidal solutions of small- and large-size Ti_3C_2 MXene flakes, which transformed traditional cellulose-based yarns into highly conductive, electrochemically and electromechanically active yarns. MXene loadings of up to 77 wt% (2.2 mg cm^{-1}) were achieved, which resulted in yarns with a remarkable electrical conductivity of up to $440.3 \pm 0.9 \text{ S cm}^{-1}$. By adjusting the stitch pattern between single jersey, half-gauge, and interlock, MXene-coated cellulose-based yarns were successfully knitted into full fabrics using an industrial knitting machine. When washed at temperatures ranging from 30 to 80 °C, the MXene loading remained almost unchanged with negligible change in the yarn resistance and conductivity. The MXene-coated cotton yarn exhibited a high length capacitance (C_L) of up to 759.5 mF cm^{-1} (2.1 mF Tex^{-1}). The C_L of 306.9 mF cm^{-1}

(0.5 mF Tex⁻¹) at 2 mV s⁻¹ was achieved when two MXene-coated cotton yarns were assembled into free-standing, symmetric yarn supercapacitor. By using the knitted MXene-coated bamboo yarns as electrodes, we achieved a textile-based capacitive pressure sensor that demonstrated a high sensitivity (GF ≈ 6.02), a sensing range of 20% compression, and excellent cycling stability at ≈ 14.1% strain for 2000 cycles. The MXene-coated yarns offer suitable properties that can meet the performance requirements of applications other than energy storage and sensing, such as triboelectric energy harvesting, EMI shielding, and heated fabrics. The established approach in this study, which combines the versatile chemistry and promising electrical and electrochemical properties of MXenes with the existing cellulose-based yarns, can offer a platform technology for various textile-based devices by allowing tunability in performance for the building blocks of textiles.

4. Experimental Section

Synthesis of Ti₃C₂T_x MXene: Ti₃AlC₂ MAX phase powder was synthesized according to the method described previously.^[33] Ti₃C₂ was synthesized by selective etching of Al atomic layers from Ti₃AlC₂ MAX phase. To prepare the MXene dispersion, 3 g of Ti₃AlC₂ was added slowly to a 60 mL of chemical etchant (6:3:1 ratio) consisting of 36 mL of 12 M hydrochloric acid (HCl, Alfa Aesar, 98.5%), 18 mL of deionized (DI) water, and 6 mL of hydrofluoric acid (HF, Acros Organics, 49.5 wt%). The mixture was stirred at 500 rpm for 24 h at room temperature. After etching, the solution was washed by repeated centrifugation at 3500 rpm for 5 min cycles. The acidic supernatant was decanted after centrifuging and DI water was then added to wash the MXene powder several times until its pH reached ≈ 5–6.

Delamination and Preparation of MXene: For delamination, 2 g of lithium chloride (LiCl, Chem-Impex Int., 99.3%) dissolved in 100 mL of DI water was added to the sediment after washing. The lithium ions intercalate between the interlayer spacings of multilayered MXene to facilitate subsequent delamination into few layered sheets. The mixture was first dispersed by manual shaking and then stirred at room temperature for 4 h. The MXene solution was then washed four times by centrifugation until the supernatant was dark, indicating delamination. To separate unreacted Ti₃AlC₂ MAX and multilayer Ti₃C₂ MXene flakes, centrifugation at 3500 rpm for 5 min was repeated. The supernatant was collected, and the sediment was redispersed with more water before beginning the next centrifuge cycle. The concentration of the MXene dispersion was measured by vacuum filtration of a known volume of solution and measuring the mass of the resulting free-standing film. To increase the concentration, the MXene dispersion was centrifuged at 9000 rpm for 2 h, the clear supernatant was decanted, and the sediment was redispersed in a known volume of DI water. The new concentration of the MXene dispersion, also called as-synthesized MXene, was measured again before being used for dip-coating. Half of the as-synthesized MXene dispersion was probe sonicated (Fisher Scientific model 505 Sonic Dismembrator, 500 W) for 20 min under a pulse setting (8 s on pulse and 2 s off pulse) at an amplitude of 50%. The MXene dispersion in a 50 mL glass bottle was inserted in an ice bath to keep the dispersion cool during sonication.

Characterization: The flake size distributions and the zeta potential measurements of the MXene dispersions were conducted using DLS. Diluted MXene dispersion was transferred into a polystyrene cuvette (Zetasizer Nano ZS, Malvern Instruments, USA), and a total of five measurements from each sample were taken for the DLS average. The weight of the yarn was measured using a scale (Mettler Toledo, Columbus, OH) before and after dip-coating to determine the MXene loading. SEM images were taken on a Zeiss Supra 50 VP with

an accelerating voltage of 3 kV to observe the MXene coating on the individual fibers and the yarn surface. Yarn cross-sections were obtained by submerging the yarn in liquid nitrogen and then manually breaking the frozen yarn. XRD was conducted to study the structure of the precursor Ti₃AlC₂ MAX, Ti₃C₂ MXene film, pristine cotton and MXene-coated cotton yarn. A Rigaku Miniflex II-Gen. 6 (Rigaku Co. Ltd. USA) with Cu K_α (λ = 0.1542 nm) source and graphite K_β filter was used for measurements and the spectra were acquired at 40 kV voltage and 15 mA current for 2θ values from 2° to 65°. AFM measurements were done using an NX-10 (Park Systems, Korea) in a standard tapping mode in air. The drive frequency was 272 kHz. The image was collected at 15 μm × 15 μm scan size at a scan rate of 0.3 Hz. AFM samples were prepared by spin-coated MXene solutions on Si/SiO₂ (300 nm) at 3000 rpm for 60 s. The substrates were then dried at 7000 rpm for 15 s. XPS was conducted using PHI VersaProbe 5000 instrument (Physical Electronics, USA) with a 200 μm and 50 W monochromatic Al-K_α (1486.6 eV) X-ray source. Charge neutralization was accomplished through a dual beam setup using low energy Ar⁺ ions and low energy electrons at 1 eV/200 μA. Sputtering on 2 mm × 2 mm area was conducted using Ar⁺-ion source at 4 kV accelerating voltage and 5 mA cm⁻² current density for up to 3 min. High-resolution Ti-2p region spectra were collected using pass energy and energy resolution of 23.5 and 0.05 eV, respectively. No binding energy scale correction was applied as the samples were conducting, charge neutralization was adequate, and no irregular shifts in the spectra were observed even after sputtering. Quantification and peak fitting were conducted using CasaXPS V2.3.19. Mixed Gaussian-Lorentzian, GL(30), peak shape was used for oxygen related moieties (TiO₂), and asymmetric Lorentzian, LA(2,4,6), was used for metal related moieties (Ti–C, Ti–O, Ti–F).

The electrical resistance of the MXene-coated yarns was measured using a two-point probe with Keysight 2400 multimeter by repeating the test on at least ten different positions. The diameter of the yarns was measured using an Olympus PMG 3 (Olympus, Center Valley, PA) optical microscope from an average of ten different locations along the yarn length. Conductivity (σ) was calculated by $\sigma = l/RA_c$, where *l*, *R*, and *A_c* are the length, resistance, and the cross-sectional area of the yarn, respectively. The mechanical properties of the MXene-coated cellulose-based yarns were analyzed using a DHR-3 (TA Instruments, DE) rheometer with a 50 N load cell and crosshead speed of 1.5 mm min⁻¹. Samples were prepared by attaching the yarn vertically onto a rectangular paper frame with 25 mm gauge length. After mounting the frame on the grips, the paper was cut in the middle and the yarn was stretched at a strain rate of 0.001 s⁻¹ (6% min⁻¹) until failure.

Knitting: The MXene-coated cellulose-based yarns were knitted using a 15-gauge, SWG041N Shima Seiki computerized knitting machine. The Apex-3 Design software was used to program knitted devices and samples. Rectangular swatches were knitted using interlock and half-gauge stitch patterns. The pressure sensor button was fully knitted from start to finish using MXene-coated bamboo yarns (0.6 mg cm⁻¹ MXene loading) as the electrode material. The sensor consists of two electrodes that were independently knitted on two separate planes (front surface and back surface). Two individual feeders, each carrying a MXene-coated bamboo yarn, were used to simultaneously knit the two independent fabric electrodes with reflective symmetry. A key consideration was to avoid contact between the two electrodes to prevent short circuiting. This was achieved by carefully designing the knitting program. After knitting of active material was completed, the machine signaled a programmed stop. The dielectric layer (nitrile rubber) was then carefully placed between the fabric electrodes and the pocket was closed by knitting a commercial viscose yarn on the subsequent row, securing the dielectric layer.

Washability: MXene-coated cotton yarns were washed with 1 mg mL⁻¹ Synthrapol solution, where they were loosely secured onto a mesh to prevent tangling during the washing process. Synthrapol is a mild detergent commonly used in yarn and fabric dyeing, which facilitates removing loose dye particles from the substrate. The MXene-coated cotton yarns fixed to the mesh were placed into a vial with the Synthrapol and stirred at 500 rpm, where the mesh was free to move

during stirring. Two sets of 100 cm long MXene-coated cotton yarns were washed for 20 washing cycles (60 min stirring for each cycle at 500 rpm) at 30 °C. Then, the same yarns (washed at 30 °C for 20 washing cycles) were further washed 5 more cycles at each listed temperature consecutively: 40, 50, 60, 70, and 80 °C. As a result, the yarns were washed 45 washing cycles in total. For each set of yarns, the MXene loading and the linear resistance along ten ≈ 1 cm long yarn segments were measured and compared. Next, the yarns were rinsed with DI and air dried at room temperature for at least 6 h and then dried in a vacuum desiccator for 4 h prior to measuring the mass loss and linear resistance.

Fabrication of Yarn Electrodes: The electrochemical properties of the MXene-coated cotton yarns were studied in a three-electrode configuration. The counter and the reference electrodes were graphite rod and Ag/AgCl (3 m KCl), respectively, and 1 m H_2SO_4 was used as the electrolyte. The working electrode was prepared by attaching an ≈ 25 –30 mm long MXene-coated cotton yarn (2.5 mg cm^{-1} of MXene loading) to the end of a fine silver wire using conductive silver paste. The connection and the silver wire were sealed using epoxy glue to avoid contact of silver paste with the electrolyte.

Fabrication of YSC Devices: For the YSC device, PVA– H_2SO_4 gel electrolyte was prepared by dissolving 3 g of PVA powder (Sigma-Aldrich, MW = 89 000–98 000) in 30 mL of water at 85 °C under vigorous stirring. 3 g of sulfuric acid (98 wt%, H_2SO_4 , Fisher Chemical) was added to the PVA solution after it cooled down to room temperature and a homogenous gel was achieved. For preparation of YSCs, MXene-coated cotton yarns (length of each yarn ≈ 60 mm) were immersed in the PVA– H_2SO_4 gel electrolyte for ≈ 10 min and dried in air overnight. The YSC device was prepared in parallel configuration by placing two MXene-coated cotton yarn electrodes next to each other and coating twice with PVA– H_2SO_4 gel electrolyte to ensure a complete coating.

Characterization of Yarn Electrodes and YSC: CV, GCD, and EIS were performed using an electrochemical workstation (VMP 3, Biologic, France) at room temperature. Yarn electrodes and devices were precycled using CV at 100 mV s^{-1} for 20 cycles prior to recording the electrochemical data. The current density values extracted in the CV and GCD curves were normalized to the length of the yarn electrode. For the three-electrode setup, CV and GCD curves were recorded at a potential window of 0.25 to -0.55 V (vs Ag/AgCl) at the scan rates ranging from 2 to 100 mV s^{-1} and at the specific current per length of 2 to 24 mA cm^{-1} , respectively. For the two-electrode setup, CV and GCD curves were recorded in a voltage window of 0 to 0.6 V at the scan rates ranging from 2 to 100 mV s^{-1} and at the specific current per length of 0.5 to 12 mA cm^{-1} . The EIS was performed at open-circuit potential within a frequency range from 1 MHz to 1 mHz at an alternating-current voltage with 10 mV amplitude. Cycling stability was measured by repeating the GCD test for 10 000 cycles at current densities of 30 and 5 mA cm^{-1} for three-electrode and two-electrode setups, respectively.

The capacitance was calculated by integrating the discharge portion of the CV data using Equation (1)

$$C_D = \frac{\int_0^t i \, dV}{v \Delta V} \quad (1)$$

where i is the instantaneous current at the potential of V , v is the scan rate (V s^{-1}), and ΔV is the potential/voltage window (V). The numerator of the equation is the integral of the discharge portion of the CV curve. The length (C_L , mF cm^{-1}), areal (C_A , mF cm^{-2}), volumetric (C_V , F cm^{-3}), and linear density (C_{Tex} , mF Tex^{-1}) specific capacitances of the electrode were obtained by normalizing the capacitance to the length, outer surface area, volume, and the linear density (Tex) of the yarn electrode, respectively (for three-electrode configuration). The specific capacitances of the supercapacitor device were calculated by normalizing the capacitance to the length of the whole device, total area, total volume, and the total linear density of the device, respectively (including both electrodes with same length).

The outer surface area (A) and volume (V) of the yarn electrode were calculated using Equations (2) and (3)

$$\text{Area} : A = 2\pi r l \quad (2)$$

$$\text{Volume} : V = \pi r^2 l \quad (3)$$

where l denotes the length of the electrode and r is the radius of the yarn electrode. The capacitance retention (C_{Ret}) of the electrode and the YSC device was calculated from the specific capacitance in the first cycle (C_1) and the specific capacitance after the cycle number i , using Equation (4)

$$C_{\text{Ret}} = \frac{C_i}{C_1} \times 100\% \quad (4)$$

Characterization of the Pressure Sensor: The pressure sensing properties of the knitted samples were measured by real-time monitoring of the capacitance response during the cyclic compression-relaxation tests. Synchronized mechanical and electrical (electromechanical) data were collected using an Instron 3300 (Model 3365, Norwood, MA) with a 100 N load cell at a crosshead speed of 5 mm min^{-1} and a multimeter (Model 34461A, Keysight, Santa Rosa, CA). Dimensions of each electrode used for the electromechanical test were $60 \text{ mm} \times 65 \text{ mm}$ in total area and $16 \text{ mm} \times 26 \text{ mm}$ in active area with a dielectric thickness of $\approx 72 \mu\text{m}$ and a total sensor thickness of $\approx 2.5 \text{ mm}$. The active area of the pressure sensor was knitted using MXene-coated bamboo yarns with 0.6 mg cm^{-1} MXene loading. The surrounding textile was knitted using a commercial viscose yarn (70 Tex). Relative capacitance change ($\Delta C/C_0$) was calculated, which represents capacitance (C) at each point normalized in respect to the initial capacitance (C_0).

Supporting Information

Supporting Information is available from the Wiley Online Library or from the author.

Acknowledgements

The research was sponsored by the Fluid Interface Reactions, Structures and Transport (FIRST) Center, an Energy Frontier Research Center (EFRC) funded by the U.S. Department of Energy, Office of Science, and Office of Basic Energy Sciences. S.S. acknowledges Endeavour Research Fellowship from the Australian Government Department of Education and Training and Alfred Deakin Postdoctoral Research Fellowship from Deakin University. A.L. and M.A. were supported by the National Science Foundation Graduate Research Fellowship under Grant No. DGE-1646737. Any opinion, findings, and conclusion or recommendations expressed in this material are those of the author(s) and do not necessarily reflect the reviews of the National Science Foundation. J.M.R. acknowledges financial support from the Australian Research Council (FT130100380). SEM, TEM, and XRD investigations were performed at the Centralized Research Facilities (CRF) at Drexel University. The authors would like to thank Kathleen Maleski (Drexel) for assistance with the Zetasizer measurements, Dr. Xu Xiao (Drexel) for TEM and SEM characterizations, and Kanit Hantanasirisakul and Deng Kuol for the AFM characterizations. Kanit Hantanasirisakul and Deng Kuol were supported by Global Research Development Center Program through the National Research Foundation of Korea (NRF) funded by the Ministry of Science and ICT (MSIT) (2015K1A4A3047100) for their internship at the National Nano Fabrication Center.

Conflict of Interest

The authors declare no conflict of interest.

Keywords

cotton, energy storage, multifunctional yarns, MXene, pressure sensor

Received: June 23, 2019

Revised: August 2, 2019

Published online:

- [1] D. Yu, K. Goh, H. Wang, L. Wei, W. Jiang, Q. Zhang, L. Dai, Y. Chen, *Nat. Nanotechnol.* **2014**, 9, 555.
- [2] D. Yu, Q. Qian, L. Wei, W. Jiang, K. Goh, J. Wei, J. Zhang, Y. Chen, *Chem. Soc. Rev.* **2015**, 44, 647.
- [3] K. Jost, G. Dion, Y. Gogotsi, *J. Mater. Chem. A* **2014**, 2, 10776.
- [4] W. Weng, P. Chen, S. He, X. Sun, H. Peng, *Angew. Chem., Int. Ed.* **2016**, 55, 6140.
- [5] Q. Xue, J. Sun, Y. Huang, M. Zhu, Z. Pei, H. Li, Y. Wang, N. Li, H. Zhang, C. Zhi, *Small* **2017**, 13, 1701827.
- [6] A. K. Yetisen, H. Qu, A. Manbachi, H. Butt, M. R. Dokmeci, J. P. Hinestroza, M. Skorobogatiy, A. Khademhosseini, S. H. Yun, *ACS Nano* **2016**, 10, 3042.
- [7] K. Jost, D. Stenger, C. R. Perez, J. K. McDonough, K. Lian, Y. Gogotsi, G. Dion, *Energy Environ. Sci.* **2013**, 6, 2698.
- [8] K. Jost, C. R. Perez, J. K. McDonough, V. Presser, M. Heon, G. Dion, Y. Gogotsi, *Energy Environ. Sci.* **2011**, 4, 5060.
- [9] M. Hu, Z. Li, G. Li, T. Hu, C. Zhang, X. Wang, *Adv. Mater. Technol.* **2017**, 2, 1700143.
- [10] J. Zhang, S. Seyedin, Z. Gu, W. Yang, X. Wang, J. M. Razal, *Nanoscale* **2017**, 9, 18604.
- [11] X. Xiao, T. Li, P. Yang, Y. Gao, H. Jin, W. Ni, W. Zhan, X. Zhang, Y. Cao, J. Zhong, L. Gong, W.-C. Yen, W. Mai, J. Chen, K. Huo, Y.-L. Chueh, Z. L. Wang, J. Zhou, *ACS Nano* **2012**, 6, 9200.
- [12] H. Yang, H. Xu, M. Li, L. Zhang, Y. Huang, X. Hu, *ACS Appl. Mater. Interfaces* **2016**, 8, 1774.
- [13] V. T. Le, H. Kim, A. Ghosh, J. Kim, J. Chang, Q. A. Vu, D. T. Pham, J.-H. Lee, S.-W. Kim, Y. H. Lee, *ACS Nano* **2013**, 7, 5940.
- [14] K. Jost, D. P. Durkin, L. M. Haverhals, E. K. Brown, M. Langenstein, H. C. de Long, P. C. Trulove, Y. Gogotsi, G. Dion, *Adv. Energy Mater.* **2015**, 5, 1401286.
- [15] M. Tebyetekerwa, I. Marriam, Z. Xu, S. Yang, H. Zhang, F. Zabihi, R. Jose, S. Peng, M. Zhu, S. Ramakrishna, *Energy Environ. Sci.* **2019**.
- [16] R. Jalili, J. M. Razal, P. C. Innis, G. G. Wallace, *Adv. Funct. Mater.* **2011**, 21, 3363.
- [17] J. Zhang, S. Seyedin, S. Qin, Z. Wang, S. Moradi, F. Yang, P. A. Lynch, W. Yang, J. Liu, X. Wang, J. M. Razal, *Small* **2019**, 15, 1804732.
- [18] J. Zhang, S. Seyedin, S. Qin, P. A. Lynch, Z. Wang, W. Yang, X. Wang, J. M. Razal, *J. Mater. Chem. A* **2019**, 7, 6401.
- [19] N. He, Q. Pan, Y. Liu, W. Gao, *ACS Appl. Mater. Interfaces* **2017**, 9, 24568.
- [20] X. Zhao, B. Zheng, T. Huang, C. Gao, *Nanoscale* **2015**, 7, 9399.
- [21] T. Xu, X. Ding, Y. Liang, Y. Zhao, N. Chen, L. Qu, *Nanoscale* **2016**, 8, 12113.
- [22] V. A. Davis, A. N. G. Parra-Vasquez, M. J. Green, P. K. Rai, N. Behabtu, V. Prieto, R. D. Booker, J. Schmidt, E. Kesselman, W. Zhou, H. Fan, W. W. Adams, R. H. Hauge, J. E. Fischer, Y. Cohen, Y. Talmon, R. E. Smalley, M. Pasquali, *Nat. Nanotechnol.* **2009**, 4, 830.
- [23] N. Behabtu, C. C. Young, D. E. Tsentelovich, O. Kleinerman, X. Wang, A. W. K. Ma, E. A. Bengio, R. F. ter Waarbeek, J. J. de Jong, R. E. Hoogerwerf, S. B. Fairchild, J. B. Ferguson, B. Maruyama, J. Kono, Y. Talmon, Y. Cohen, M. J. Otto, M. Pasquali, *Science* **2013**, 339, 182.
- [24] Q. Meng, H. Wu, Y. Meng, K. Xie, Z. Wei, Z. Guo, *Adv. Mater.* **2014**, 26, 4100.
- [25] M.-Q. Zhao, C. E. Ren, Z. Ling, M. R. Lukatskaya, C. Zhang, K. L. van Aken, M. W. Barsoum, Y. Gogotsi, *Adv. Mater.* **2015**, 27, 339.
- [26] S. Seyedin, E. R. S. Yanza, J. M. Razal, *J. Mater. Chem. A* **2017**, 5, 24076.
- [27] S. Seyedin, J. M. Razal, P. C. Innis, A. Jeiranikhameneh, S. Beirne, G. G. Wallace, *ACS Appl. Mater. Interfaces* **2015**, 7, 21150.
- [28] T. Chen, L. Qiu, Z. Yang, Z. Cai, J. Ren, H. Li, H. Lin, X. Sun, H. Peng, *Angew. Chem., Int. Ed.* **2012**, 51, 11977.
- [29] Z. Wang, S. Qin, S. Seyedin, J. Zhang, J. Wang, A. Levitt, N. Li, C. Haines, R. Ovalle-Robles, W. Lei, Y. Gogotsi, R. H. Baughman, J. M. Razal, *Small* **2018**, 14, 1802225.
- [30] M. D. Lima, S. Fang, X. Lepró, C. Lewis, R. Ovalle-Robles, J. Carretero-González, E. Castillo-Martínez, M. E. Kozlov, J. Oh, N. Rawat, C. S. Haines, M. H. Haque, V. Aare, S. Stoughton, A. A. Zakhidov, R. H. Baughman, *Science* **2011**, 331, 51.
- [31] C. Zhang, B. Anasori, A. Seral-Ascaso, S.-H. Park, N. McEvoy, A. Shmeliov, G. S. Duesberg, J. N. Coleman, Y. Gogotsi, V. Nicolosi, *Adv. Mater.* **2017**, 29, 1702678.
- [32] M. R. Lukatskaya, S. Kota, Z. Lin, M.-Q. Zhao, N. Shpigel, M. D. Levi, J. Halim, P.-L. Taberna, M. W. Barsoum, P. Simon, Y. Gogotsi, *Nat. Energy* **2017**, 2, 17105.
- [33] M. Alhabeb, K. Maleski, B. Anasori, P. Lelyukh, L. Clark, S. Sin, Y. Gogotsi, *Chem. Mater.* **2017**, 29, 7633.
- [34] M. R. Lukatskaya, O. Mashtalir, C. E. Ren, Y. Dall'Agnese, P. Rozier, P. L. Taberna, M. Naguib, P. Simon, M. W. Barsoum, Y. Gogotsi, *Science* **2013**, 341, 1502.
- [35] Z. Ling, C. E. Ren, M.-Q. Zhao, J. Yang, J. M. Giammarco, J. Qiu, M. W. Barsoum, Y. Gogotsi, *Proc. Natl. Acad. Sci. USA* **2014**, 111, 16676.
- [36] M. D. Levi, M. R. Lukatskaya, S. Sigalov, M. Beidaghi, N. Shpigel, L. Daikhin, D. Aurbach, M. W. Barsoum, Y. Gogotsi, *Adv. Energy Mater.* **2015**, 5, 1400815.
- [37] M. R. Lukatskaya, S.-M. Bak, X. Yu, X.-Q. Yang, M. W. Barsoum, Y. Gogotsi, *Adv. Energy Mater.* **2015**, 5, 1500589.
- [38] H. Lin, X. Wang, L. Yu, Y. Chen, J. Shi, *Nano Lett.* **2017**, 17, 384.
- [39] F. Meng, M. Seredych, C. Chen, V. Gura, S. Mikhalevsky, S. Sandeman, G. Ingavle, T. Ozulumba, L. Miao, B. Anasori, Y. Gogotsi, *ACS Nano* **2018**, 12, 10518.
- [40] K. Maleski, C. E. Ren, M.-Q. Zhao, B. Anasori, Y. Gogotsi, *ACS Appl. Mater. Interfaces* **2018**, 10, 24491.
- [41] V. S. Smentkowski, *Prog. Surf. Sci.* **2000**, 64, 1.
- [42] T. Habib, X. Zhao, S. A. Shah, Y. Chen, W. Sun, H. An, J. L. Lutkenhaus, M. Radovic, M. J. Green, *npj 2D Mater. Appl.* **2019**, 3, 8.
- [43] Y. Chae, S. J. Kim, S.-Y. Cho, J. Choi, K. Maleski, B.-J. Lee, H.-T. Jung, Y. Gogotsi, Y. Lee, C. W. Ahn, *Nanoscale* **2019**, 11, 8387.
- [44] C. J. Zhang, S. Pinilla, N. McEvoy, C. P. Cullen, B. Anasori, E. Long, S.-H. Park, A. Seral-Ascaso, A. Shmeliov, D. Krishnan, C. Morant, X. Liu, G. S. Duesberg, Y. Gogotsi, V. Nicolosi, *Chem. Mater.* **2017**, 29, 4848.
- [45] G.-M. Weng, J. Li, M. Alhabeb, C. Karpovich, H. Wang, J. Lipton, K. Maleski, J. Kong, E. Shaulsky, M. Elimelech, Y. Gogotsi, A. D. Taylor, *Adv. Funct. Mater.* **2018**, 28, 1803360.
- [46] D. Xiong, X. Li, Z. Bai, S. Lu, *Small* **2018**, 14, 1703419.
- [47] M. Ghidui, M. R. Lukatskaya, M.-Q. Zhao, Y. Gogotsi, M. W. Barsoum, *Nature* **2014**, 516, 78.
- [48] M. Beidaghi, Y. Gogotsi, *Energy Environ. Sci.* **2014**, 7, 867.
- [49] M. D. Stoller, R. S. Ruoff, *Energy Environ. Sci.* **2010**, 3, 1294.
- [50] A. W. Bayes, *J. Text. Inst. Proc.* **1957**, 48, 255.
- [51] L. Liu, Y. Yu, C. Yan, K. Li, Z. Zheng, *Nat. Commun.* **2015**, 6, 7260.
- [52] N. Liu, W. Ma, J. Tao, X. Zhang, J. Su, L. Li, C. Yang, Y. Gao, D. Golberg, Y. Bando, *Adv. Mater.* **2013**, 25, 4925.

- [53] C. Jin, H.-T. Wang, Y.-N. Liu, X.-H. Kang, P. Liu, J.-N. Zhang, L.-N. Jin, S.-W. Bian, Q. Zhu, *Electrochim. Acta* **2018**, 270, 205.
- [54] Y.-Y. Peng, B. Akuzum, N. Kurra, M.-Q. Zhao, M. Alhabeab, B. Anasori, E. C. Kumbur, H. N. Alshareef, M.-D. Ger, Y. Gogotsi, *Energy Environ. Sci.* **2016**, 9, 2847.
- [55] N. Kurra, B. Ahmed, Y. Gogotsi, H. N. Alshareef, *Adv. Energy Mater.* **2016**, 6, 1601372.
- [56] X. Wang, T. S. Mathis, K. Li, Z. Lin, L. Vlcek, T. Torita, N. C. Osti, C. Hatter, P. Urbankowski, A. Sarycheva, M. Tyagi, E. Mamontov, P. Simon, Y. Gogotsi, *Nat. Energy* **2019**, 4, 241.
- [57] J. Lee, H. Kwon, J. Seo, S. Shin, J. H. Koo, C. Pang, S. Son, J. H. Kim, Y. H. Jang, D. E. Kim, T. Lee, *Adv. Mater.* **2015**, 27, 2433.
- [58] D. J. Lipomi, M. Vosgueritchian, B. C. K. Tee, S. L. Hellstrom, J. A. Lee, C. H. Fox, Z. Bao, *Nat. Nanotechnol.* **2011**, 6, 788.